Journal of Integrative Neuroscience

J. Integr. Neurosci. **2023**; 22(4): 101
https://doi.org/10.31083/j.jin2204101

Original Research

Diffusion tensor imaging (DTI) Analysis Based on Tract-based spatial statistics (TBSS) and Classification Using Multi-Metric in Alzheimer's Disease

Yingteng Zhang[1], Feibiao Zhan[2,*]

[1]Department of Mathematics, Taizhou University, 225300 Taizhou, Jiangsu, China
[2]Department of Applied Mathematics, Nanjing Audit University, 211815 Nanjing, Jiangsu, China
*Correspondence: zhanfeibiao@yeah.net (Feibiao Zhan)

Academic Editor: Gernot Riedel
Submitted: 12 November 2022 Revised: 14 January 2023 Accepted: 17 January 2023 Published: 20 July 2023

Abstract

Background: Alzheimer's disease (AD) is a brain disorder characterized by atrophy of cerebral cortex and neurofibrillary tangles. Accurate identification of individuals at high risk of developing AD is key to early intervention. Combining neuroimaging markers derived from diffusion tensor images with machine learning techniques, unique anatomical patterns can be identified and further distinguished between AD and healthy control (HC). **Methods**: In this study, 37 AD patients (ADs) and 36 healthy controls (HCs) from the Alzheimer's Disease Neuroimaging Initiative were applied to tract-based spatial statistics (TBSS) analysis and multi-metric classification research. **Results**: The TBSS results showed that the corona radiata, corpus callosum and superior longitudinal fasciculus were the white matter fiber tracts which mainly suffered the severe damage in ADs. Using support vector machine recursive feature elimination (SVM-RFE) method, the classification performance received a decent improvement. In addition, the integration of fractional anisotropy (FA) + mean diffusivity (MD) + radial diffusivity (RD) into multi-metric could effectively separate ADs from HCs. The rank of significance of diffusion metrics was FA > axial diffusivity (DA) > MD > RD in our research. **Conclusions**: Our findings suggested that the TBSS and machine learning method could play a guidance role on clinical diagnosis.

Keywords: Alzheimer's disease; diffusion tensor imaging; diffusion metric; tract-based spatial statistics; support vector machine; classification

1. Introduction

Alzheimer's disease (AD) is associated with abnormal functioning of the nervous system and usually appears in people over the age of 60. Patients are often accompanied by memory loss and cognitive decline and other problems, which not only seriously harms the physical and mental health of patients, but also brings a heavy burden on families and society [1]. It is estimated that in 30 years there will be 134.6 million cases of AD worldwide [2]. However, the exact cause of AD is still unknown and existing targeted drugs can only reduce symptoms or delay its progression. Therefore, revealing the brain changes caused by the disease is crucial to explore the underlying cause of AD [3].

Precise diagnosis of AD helps patients improve future quality of life, including early prevention and optimal treatment [4]. With the fast development of artificial intelligence and medical imaging technology, computer-aided diagnosis provides sufficient evidence of accuracy to distinguish AD from healthy control (HC) [5–10]. Traditionally, AD has been thought of as a disease of gray matter (GM) damage, while the effects of white matter (WM) have generally been thought of as damage secondary to GM [11]. Although there is growing concern about WM damage in AD, our knowledge is still limited when compared to GM atrophy and other biomarkers. In particular, a review illustrates different main research point of penetration for how WM injury leads to AD [12]. One piece of evidence is to study WM degeneration and demyelination as the important pathophysiological features of AD at the microstructural level [13,14]. Another piece of evidence comes from neuroimaging, which have the remarkable advantage of being able to noninvasively observe morphologic changes in patients' brains. Despite the study is focused on WM microstructures, it's important to highlight that diffusion tensor imaging (DTI) can be used to investigate even microstructural changes in GM (not only WM) [15,16]. With the development of DTI technology, it can be used to show the direction of fasciculus in the WM of the brain, which is the only non-invasive imaging method that can show the fasciculus *in vivo* [17].

There are some common metrics that can reflect the brain microstructure in DTI, such as fractional anisotropy (FA), mean diffusivity (MD), axial diffusivity (DA) and radial diffusivity (RD). FA represents the directivity of water molecular dispersion and can reflect the maximum possible arrangement direction of WM tracts. The FA value is higher in WM, close to 1, while it is close to 0 in cerebrospinal fluid. MD represents the overall dispersion of water molecules. DA represents the degree of dispersion

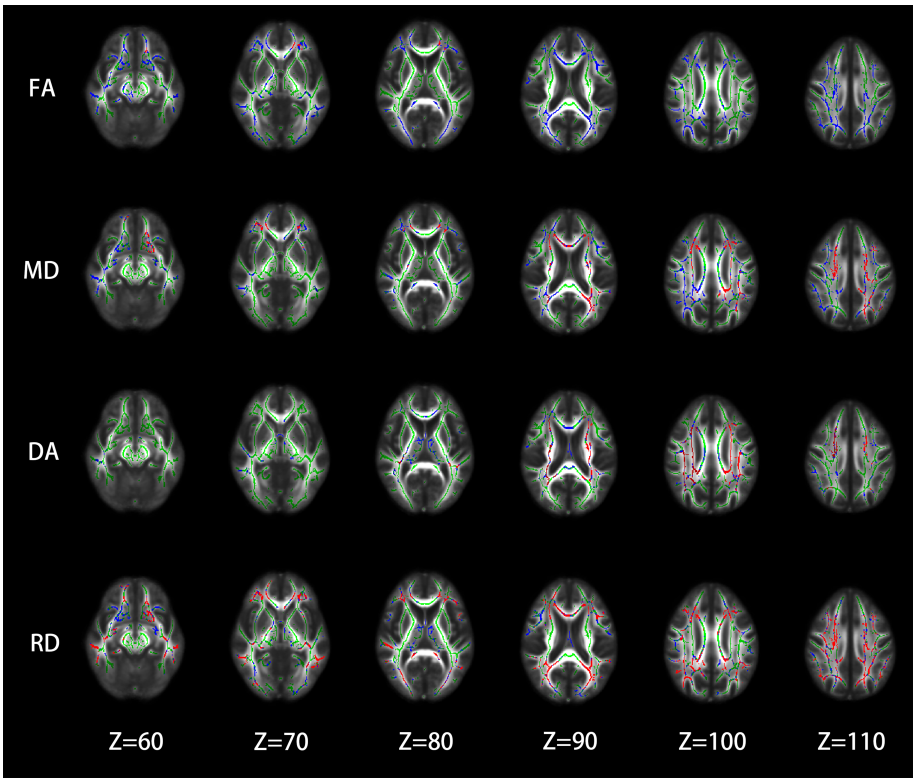

Fig. 1. The TBSS images of the DTI metrics (i.e., FA, MD, DA, RD) in horizontal slices of brain. Each column represents the different Z-axis value from Z = 60 to Z = 110. Significantly decreased FA and significantly increased MD, DA, RD in ADs versus HCs (Green: the skeleton, Blue: $p < 0.05$ with FWE corrected, red: $p < 0.01$ with FWE corrected). FA, fractional anisotropy; MD, mean diffusivity; DA, axial diffusivity; RD, radial diffusivity; TBSS, Tract-based spatial statistics; DTI, Diffusion tensor imaging; AD, Alzheimer's disease; HC, healthy control, FWE, family-wise error.

of water molecules along the main direction. RD represents the dispersion of water molecules in the other two directions [18,19]. For further understand the pathological mechanisms of WM tracts' change, tract-based spatial statistics (TBSS) method has been applied to research the microstructural of WM [20]. In recent years, machine learning-based neuroimaging technology for AD diagnosis and disease development has become a research hotspot [21–24]. As a widely used supervised learning method, support vector machine (SVM) shows good advantages in solving small sample, nonlinear and high-dimensional pattern recognition problems [25–28].

Here, we aimed to analyze research microstructural difference of WM and predict the accuracy between ADs and HCs. Therefore, the TBSS and SVM method will be used in our study. Specifically, we combined with different kind of DTI metric together for improving classification performance and rank the importance of the WM fiber tract.

2. Materials and Methods

2.1 Subjects

A total of 73 subjects from Alzheimer's Disease Neuroimaging Initiative Grand Opportunities/phase 2 (ADNI-GO/2) database (http://adni.loni.usc.edu/) [29] were collected for this study. As everyone knows, the ADNI dataset has the multi-site nature which characterized by different scanners and acquisition protocols, can have an impact on DTI data such as noise and bias. However, harmonization methods already applied on ADNI DTI data in other studies [30,31] could fix this issue in the future. Before scanning, the subjects undergo cognitive and behavioral assessments. Statistical analysis of basic information in Table 1 is completed in SPSS 22.0 (IBM Corp., Armonk, NY, USA). The Table 1 display *p*-values and t-value for two sample *t*-tests for each sample characteristic except for gender, which displays *p*-values and chi square value from a Chi square test.

2.2 Image Acquisition

All subjects are scanned through a 3T GE MEDICAL SYSTEMS scanner (General Electric company, Boston, MA, USA). A whole brain diffusion MRI (dMRI) SE-EPI (spin-echo echo-planar imaging) is acquired with the following parameters: echo time (TE): 68.3 ms, repetition time (TR): 13,000 ms, Slice Thickness: 2.7 mm, Field Strength: 3.0, Flip Angle: 90 degree, 128 mm $\times$ 128 mm matrix size, b-value: 1000 s/mm^2 (41 non-collinear directions) and 5 images with no diffusion weighting.

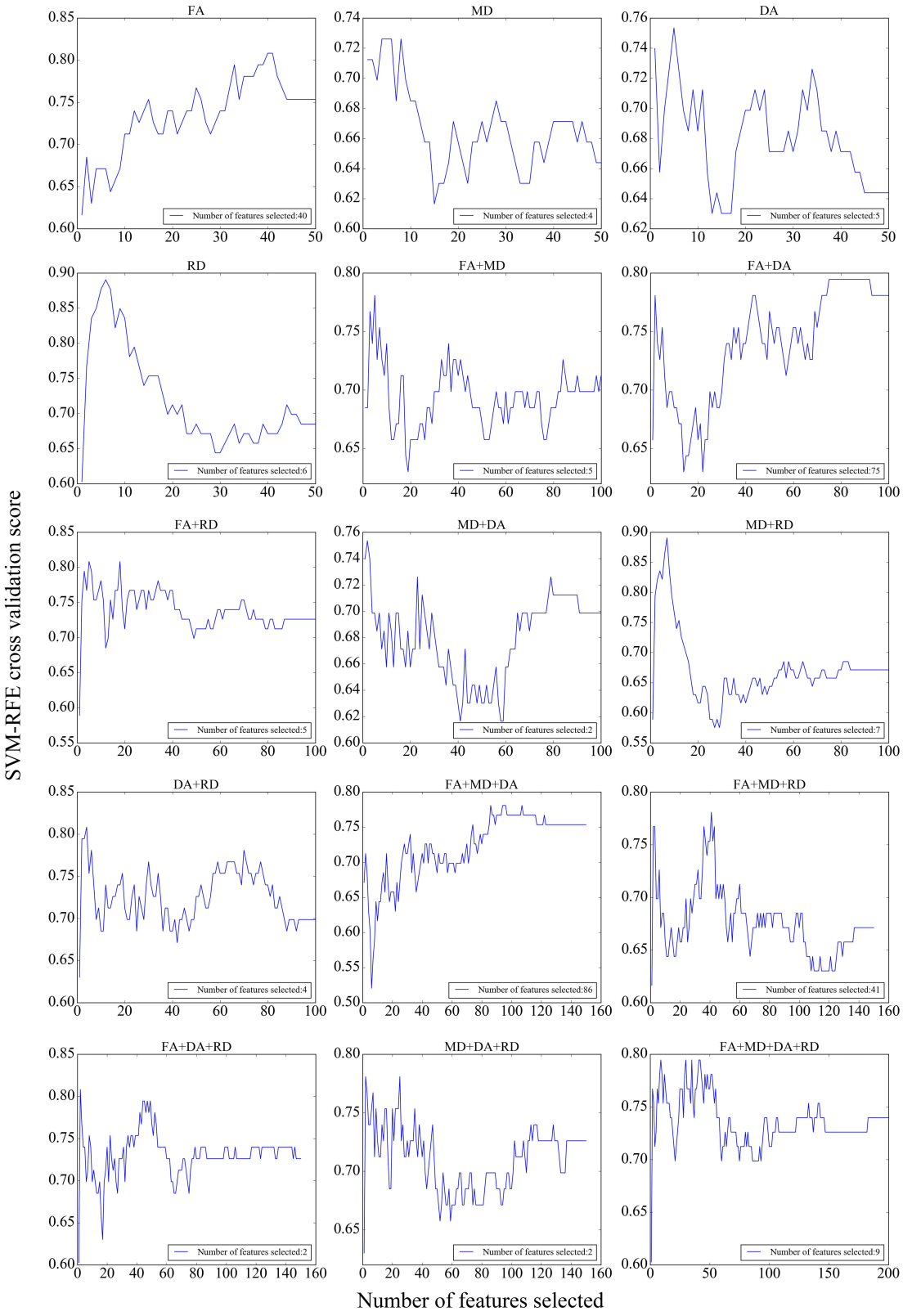

Fig. 2. Feature ranking with SVM-RFE and LOOCV selection of the best number of features. Each subgraph represented the cross validation score corresponding to the number of features selected for 15 kinds of single metric or multi-metric. The best feature dimensions are shown in a rectangular box at the bottom right of each subgraph for each kind of diffusion metrics. SVM-RFE, support vector machine recursive feature elimination; LOOCV, leave-one-out cross validation.

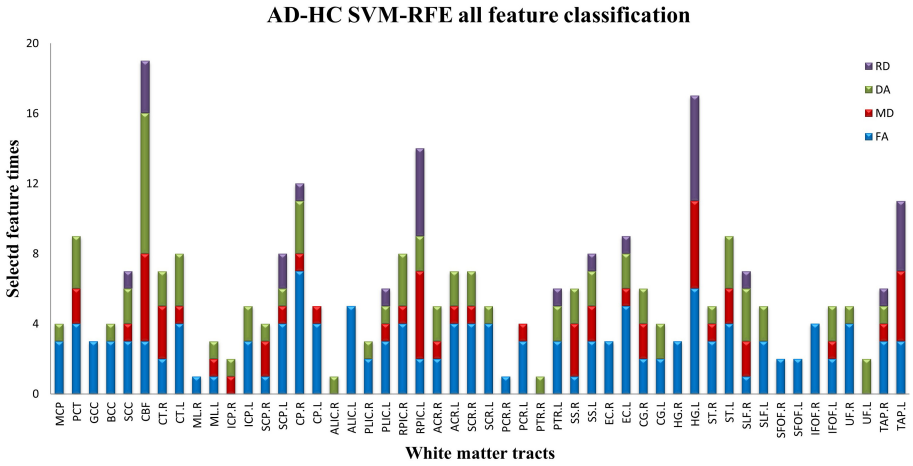

Fig. 3. The feature weighting distribution of WM tracts received by the summation of all combined approaches. WM, white matter.

Table 1. Demographic characteristics of the ADs and HCs.

	ADs (n = 37)	HCs (n = 36)	*p*-value	Chi2/ t-value
Gender (male:female)	25:12	19:17	0.197	1.667
Age (years)	74.81 ± 8.99	73.28 ± 6.19	0.398	0.85
MMSE	23.38 ± 1.98	28.81 ± 1.56	<0.001	–12.984
CDR	4.55 ± 1.43	0.03 ± 0.12	<0.001	19.153

Data is mean ± standard deviation. Columns on the right display *p*-values and t-value for two sample *t*-tests for each sample characteristic except for gender, which displays *p*-values and chi square value from a Chi square test. MMSE, Mini-Mental State Examination; CDR, Clinical Dementia Rating; AD, Alzheimer's disease; HC, healthy control.

2.3 Data Processing

Currently, PANDA (A Pipeline for Analysing Brain Diffusion Images) [32] is commonly used to process DTI data. PANDA software package is based on Linux operating system (Ubuntu 21.04, Canonical, London, UK) and Matlab software (MATLAB 9.7, MathWorks, Natick, MA, USA). In addition, PANDA's underlying commands invoke Functional magnetic resonance imaging of the brain (FMRIB) Software Library (FSL) tools [33], Diffusion Toolkit [34], Pipeline System for Octave and Matlab (PSOM) [35], and MRIcron tools (https://people.cas.sc.edu/rorden/mricron/install.html). The preprocessing steps mainly include: (1) converting Digital Imaging and Communications in Medicine (DICOM) data to Neuroimaging Informatics Technology Initiative (NIFTI) format; (2) head movement and eddy current correction; (3) brain tissue was removed by Brain Extraction Tool (BET); (4) DTI metrics (i.e., FA, MD, DA, RD) calculation with non-linear fitting algorithm.

2.4 TBSS Analysis

The tract-based spatial statistics (TBSS) can fully reflect the microstructural changes of the whole brain WM and the skeletonized data processing method can obtain high accuracy without smoothing [20]. All subjects' FA maps were nonlinearly aligned to a 1 × 1 × 1 mm standard space in Montreal Neurological Institute (MNI152) coordinates, using FSL FNIRT and FMRIB58_FA as template image. A template skeleton derived from the FMRIB58_FA (50 core regions are listed in Table 2 (Ref. [36])) was used for the analysis. This skeleton set a thresholds with 0.2 and individual FA data were projected into it for every subject. According to the standard TBSS workflow, data were entered into voxel-wise statistics to test for the group comparisons: HCs versus. ADs. The tool "randomize" was utilized by setting 5000 permutations and statistical threshold of $p < 0.05$ or $p < 0.01$. The threshold-free cluster enhancement (TFCE) was adopted as a correction for multiple comparisons. The result of comparison among groups of each parameter diagram overlaid on the FMRIB58_FA template via FSLEYES tool and used the WM tracts atlas carried by FSL for recognizing the discrepant area which had statistical significance. In addition, in order to visually view the discrepant condition of the same WM tract between groups, the TBSS mapping had converted to corresponding cluster size table via cluster locater tool in PANDA.

2.5 SVM Method and Analysis

The machine learning algorithm used in this study comes from Python's scikit-learn library [37]. The present application demonstrates that SVM was very good at mining information features [38]. Different type of SVM such as linear, non-linear with different kernel, SVM with recursive feature elimination (RFE) or regularization were applied to classify different disorders. In this paper, linear support vector machine recursive feature elimination (SVM-RFE) [39] was used to obtain the feature weight

Table 2. The rICBM-DTI-81 White Matter Parcellation Map (WMPM) FMRIB58 atlas.

rICBM-DTI-81 WMPM FMRIB58 atlas [36]			
Middle cerebellar peduncle	MCP	Pontine crossing tract	PCT
Splenium of corpus callosum	SCC	Column and body of fornix	CBF
Genu of corpus callosum	GCC	Body of corpus callosum	BCC
Medial lemniscus.R	ML.R	Medial lemniscus.L	ML.L
Corticospinal tract.R	CT.R	Corticospinal tract.L	CT.L
Superior cerebellar peduncle.R	SCP.R	Superior cerebellar peduncle.L	SCP.L
Inferior cerebellar peduncle.R	ICP.R	Inferior cerebellar peduncle.L	ICP.L
Cerebral peduncle.R	CP.R	Cerebral peduncle.L	CP.L
Posterior limb of internal capsule.R	PLIC.R	Posterior limb of internal capsule.L	PLIC.L
Anterior limb of internal capsule.R	ALIC.R	Anterior limb of internal capsule.L	ALIC.L
Retrolenticular part of internal capsule.R	RPIC.R	Retrolenticular part of internal capsule.L	RPIC.L
Posterior thalamic radiation.R	PTR.R	Posterior thalamic radiation.L	PTR.L
Superior corona radiata.R	SCR.R	Superior corona radiata.L	SCR.L
Anterior corona radiata.R	ACR.R	Anterior corona radiata.L	ACR.L
Posterior corona radiata.R	PCR.R	Posterior corona radiata.L	PCR.L
External capsule.R	EC.R	External capsule.L	EC.L
Sagittal stratum.R	SS.R	Sagittal stratum.L	SS.L
Hippocampus gyrus.R	HG.R	Hippocampus gyrus.L	HG.L
Cingulate gyrus.R	CG.R	Cingulate gyrus.L	CG.L
Stria terminalis.R	ST.R	Stria terminalis.L	ST.L
Superior fronto-occipital fasciculus.R	SFOF.R	Superior fronto-occipital fasciculus.L	SFOF.L
Superior longitudinal fasciculus.R	SLF.R	Superior longitudinal fasciculus.L	SLF.L
Uncinate fasciculus.R	UF.R	Uncinate fasciculus.L	UF.L
Inferior fronto-occipital fasciculus.R	IFOF.R	Inferior fronto-occipital fasciculus.L	IFOF.L
Tapetum.R	TAP.R	Tapetum.L	TAP.L

ranking that could best distinguished ADs and HCs. The SVM-RFE method could gradually minimize superfluous and irrelevant features [40]. The SVM-RFE method eliminated useless features one by one during each recursive process and had been successfully applied to feature selection in several functional neuroimaging studies [41,42]. In addition, the leave-one-out cross validation (LOOCV) method was used for cross validation [43]. In this process, for each selected number of features, N classifications were made (where N corresponds to the number of subjects). The mean value of N classification accuracies was similar to the classification accuracy of corresponding feature numbers in the training data set.

The result of classification is the mean accuracy, sensitivity and specificity. Sensitivity is the percentage of samples that are actually positive that are judged to be positive. It is calculated as the ratio of true positive (TP) divided by true positive (TP) + false negative (FN) (actually positive but judged negative). Specificity refers to the proportion of samples that are actually negative that are judged to be negative. It is calculated as the ratio of true negative (TN) divided by true negative (TN) + false positive (FP) (actually negative but judged positive). Accuracy is expressed by the percentage of the total number of TP and TN in the number of subjects. For a more complete understanding of the classifier's performance, sensitivity, specificity, and overall accuracy should be reported. Another very common method of reporting binary classifier results is to plot a receiver operating characteristic (ROC) curve [44]. ROC curve is a complete image of classifier performance provided by setting classification threshold value, in which, the horizontal coordinate represents false positive rate (FPR) (i.e., 1-specificity), and the vertical coordinate represents true positive rate (TPR), i.e., sensitivity. It is always desirable to have a numerical value to indicate whether a classifier is good or bad. The area under ROC curve (AUC) is the size of the area below the ROC curve. Typically, AUC values range from 0 to 1, with a larger AUC representing better performance. AUC is a standard used to measure the quality of a classification model [45].

3. Results

3.1 Statistical Analysis

There are no significant differences ($p > 0.05$) in age and sex between ADs and HCs (See Table 1 for group characteristics). It shows that ADs have a lower score of Mini-Mental State Examination (MMSE) but higher score of Clinical Dementia Rating (CDR) than HCs. The gender and age were regressed as covariables.

As shown in Fig. 1 and Table 3, compared with HC group, FA values of several WM regions in AD group de-

creased, and the WM fiber with the most significant difference was ACR.L (cluster number >100, $p < 0.01$, FWE corrected).

Table 3. Difference of diffusion metrics of the WM tracts distribution in ADs versus HCs.

WM tracts	ADs versus HCs cluster size			
	FA	MD	DA	RD
GCC	967	993*	670	1072*
BCC	1507	2163*	1367*	2299*
SCC	2063	2155*	1553*	2428*
CBF	-	-	140	140
CP.R	299	-	-	189*
ALIC.L	-	151	175	-
PLIC.R	264	169	184*	136
PLIC.L	-	178	216*	-
RPIC.R	-	-	393*	-
RPIC.L	-	-	237*	-
ACR.R	958	1251*	520*	1328*
ACR.L	1095*	1329*	444*	1414*
SCR.R	475	1520*	1472*	1014*
SCR.L	234	1390*	1292*	681*
PCR.R	388	650	671*	539*
PCR.L	121	538*	608*	349*
PTR.R	721	186	167	673*
PTR.L	636	389*	197*	674*
SS.R	211	229	-	293*
SS.L	205	191	-	402*
EC.L	-	169	113	-
CG.R	296	199	-	288
CG.L	-	129	-	-
HG.R	175	-	-	175*
ST.R	176	-	-	178*
ST.L	199	-	-	193*
SLF.R	773	1460	1028*	1288*
SLF.L	472	1161*	974*	1012*
IFOF.R	117	213	-	183
IFOF.L	106	260*	-	255*

Note: The numerical value showed above represent the cluster number >100, $p < 0.05$, FWE corrected. The numerical value marked with an asterisk (*) represent the cluster number >100, $p < 0.01$, FWE corrected. WM, white matter; FA, fractional anisotropy; MD, mean diffusivity; DA, axial diffusivity; RD, radial diffusivity.

Similarly, compared with HC group, MD values of several WM regions in AD group increased, and the WM fiber with the most significant difference were GCC, BCC, SCC, bilateral ACR, bilateral SCR, PCR.L, PTR.L, SLF.L, IFOF.L (cluster number >100, $p < 0.01$, FWE corrected).

Similarly, compared with HC group, DA values of several WM regions in AD group increased, and the WM fiber with the most significant difference were BCC, SCC, bilateral PLIC, bilateral RPIC, bilateral ACR, bilateral SCR, bilateral PCR, PTR.L, bilateral SLF (cluster number >100, $p < 0.01$, FWE corrected).

Similarly, compared with HC group, RD values of several WM regions in AD group increased, and the WM fiber with the most significant difference were GCC, BCC, SCC, CP.R, bilateral ACR, bilateral SCR, bilateral PCR, bilateral PTR, bilateral SS, HG.R, bilateral ST, bilateral SLF, IFOF.L (cluster number >100, $p < 0.01$, FWE corrected).

3.2 Feature Selection and Classification Accuracy

The best number of features of 15 kinds of single metric or multi-metric had been drawn in the corresponding rectangular frame through the SVM-RFE and LOOCV. The X-axis value corresponding to the curve peak value was the best feature dimension.

Combined with Fig. 2 and Table 4, it could be found that FA+MD+RD received the highest accuracy which increased from 67.12% to 100% among all kinds of DTI metrics while its optimal feature dimension was not the minimum. Through SVM-RFE approach, the accuracy, sensitivity and specificity of classification received some measure of improvement. For some kinds of multi-metric, the penalty factors had been adjusted which marked with an asterisk in order to improve the classifying quality.

In order to investigate the weight distribution of different WM tract and the percent of different DTI metric on each WM tract, Fig. 3 was computed to depict the WM tract for which could classify the ADs from HCs.

These ROC curves in Fig. 4 showed the classifier performance of different kind of DTI metric combined approach, computed from 5-fold cross-validation. Taking all of these curves, it was possible to calculate the AUC, and intuitively find the improvement of the classifier output performance. From above it could be found that the ROC curve which computed from FA+MD+RD received a high classifier output quality since it had a perfect AUC.

4. Discussion

In our study, two aspects were mainly researched: statistical analysis of DTI data and classification. The subjects were firstly preprocessed using PANDA tool. Then the statistical analysis was operated by TBSS and classification process was conducted by SVM method.

Relevant literatures showed that the association fiber and limbic system were the most reported abnormal regions in the WM tracts of AD [46–48]. Cingulate was the association fiber between cingulate gyrus and other brain structures. Its integrity might directly relate to the emotion and cognitive function in AD patients. In our study, FA value of the right cingulate gyrus in ADs obviously decreased compared to HCs that was agreed with previous researches [49,50]. In addition, association fiber contacted with part cortex of the ipsilateral hemisphere, FA value of bilateral sagittal stratum, superior fronto-occipital fasciculus and superior longitudinal fasciculus in ADs decreased

Table 4. Classification accuracy, sensitivity and specificity of multiple diffusion metrics.

Diffusion metrics	Optimal feature dimensions	Accuracy/%		Sensitivity/%		Specificity/%	
		Before	After	Before	After	Before	After
FA	40	75.34	89.04	75.68	89.19	75.00	88.89
MD	4	64.38	79.45	65.71	78.95	63.16	80.00
DA	5	64.38	82.19	65.71	83.33	63.16	81.08
RD	6	68.49	91.78	66.67	91.89	70.97	91.67
FA + MD	5	71.23	86.30*	72.22	90.91*	70.27	82.5*
FA + DA	75	78.08	90.41	78.38	94.12	77.78	87.18
FA + RD	5	72.60	89.04	71.79	89.19	73.53	88.89
MD + DA	2	69.86	79.45	71.43	82.35	68.42	76.92
MD + RD	7	67.12	93.15	66.67	94.44	67.65	91.89
DA + RD	4	69.86	87.67	71.43	88.89	68.42	86.49
FA + MD + DA	86	75.34	93.15	77.14	97.06	73.68	89.74
FA + MD + RD	41	67.12	100	66.67	100	67.65	100
FA + DA + RD	2	72.60	83.56*	74.29	87.88*	71.05	80*
MD + DA + RD	2	72.60	79.45	75.76	82.35	70.00	76.92
FA + MD + DA + RD	9	73.97	91.78*	76.47	97.06*	71.79	87.5*

The numerical value marked with an asterisk (*) represent a parameter optimization: FA + MD: C = 0.1; FA + DA + RD: C = 0.02; FA + MD + DA + RD: C = 0.1. The default C value is 1 and C represent penalty factor.

compared with HCs that was agreed with Teipel's research [51]. Correlational study found superior fronto-occipital fasciculus influenced visual spatial processing and memory function [52]. The damage of superior longitudinal fasciculus might involve spatial working memory and linguistic function [53]. The decrease of these functions was reflected on ADs than related to our research results. Optic radiation was the central neurons of visual pathway so that its lesion would lead to defect of field vision. In our study, decrease of FA value of posterior thalamic radiation in ADs hinted the damage of visual performance [54]. Wang *et al.* [55] based on TBSS with multi-parameter found that bilateral hippocampus gyrus existed obvious abnormal in ADs and patients with mild cognitive impairment (MCIs), including the decrease of FA value and increase of RD value, especially the right hemisphere in which was most significant. While our study found the difference just exists in the right hippocampus gyrus. MD value increased when the tissue damage. Increased MD and decreased FA were found in the corpus callosum that was agreed with previous research [56]. The corpus callosum was a bundle of fibers connecting the right and left hemispheres of the brain. On the basis of previous researches, the anterior part of the corpus callosum was connected to the prefrontal cortex and was associated with the sense of motivation [57].

Therefore, our results suggested that communication disorders between brain structures might be related to apathy symptoms of ADs [58,59]. Moreover, the particular pattern of association between severity of apathy and corpus callosum integrity might reflect slower initiation and longer response times for tasks involving hemispheric metastasis or interregional integration in apathetic ADs. Previous results had demonstrated increased MD in most lobar regions of ADs, including frontal lobes [56], temporal lobes [56], parietal lobes [60], and occipital lobe [60]. DA and RD also increased in addition to FA and MD. However, the relevant research for DA and RD was little. Our findings suggested that DA and RD might be a useful biomarker in identifying HCs and ADs.

After the SVM-RFE method, each kind of DTI metric received the optimal feature dimensions that listed in Table 4. Obviously, the majority of diffusion metrics received optimal effect after dimensionality reduction. In addition, the accuracy, sensitivity and specificity of each kind of diffusion metrics were improved via the SVM-RFE method. Several kinds of multi-metrics were further improved by adjusting the penalty factor C value. Table 4 showed that the FA+MD+RD metric received the best classification accuracy. For further investigated the effect of feature weighting on classification performance, Fig. 3 had been drawn to show the feature weighting distribution of WM tracts by the summation of all combined approaches. The feature weighting of CBF, HG.L and RPIC.L exceed 0.6 while that of ML.R, ALIC.R and PCR.R almost zero. It was also found that the rank of significance of diffusion metrics was FA $>$ DA $>$ MD $>$ RD. In order to visually evaluate classifier output quality, The ROC curve and AUC were depicted from before and after the dimension reduction. Fig. 4 showed that the AUC increased after the SVM-RFE method. The results ulteriorly verified the effectiveness of the dimension reduction.

5. Conclusions

In this paper, we introduced multi-metrics measures to identify the difference between HCs and ADs based on TBSS method. The corona radiata, corpus callosum and

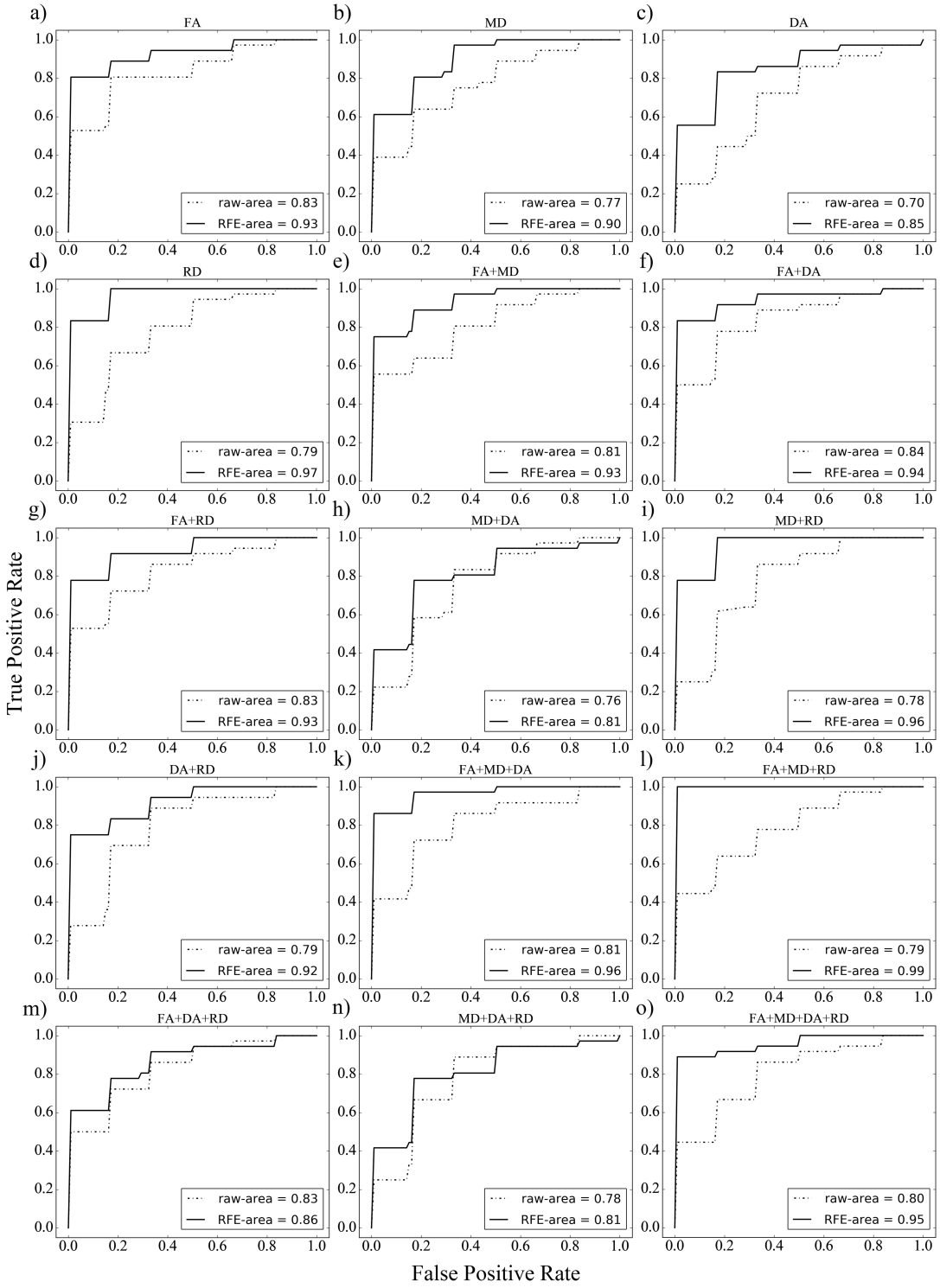

Fig. 4. Different DTI metric of ROC curve to evaluate classifier performance by 5-fold cross-validation. The ROC curve with dotted line represented the AUC before SVM-RFE and the ROC curve with solid line represented the AUC after SVM-RFE. (a–o) represented the ROC curve and AUC for 15 kinds of DTI metric through combined approach, respectively. ROC, receiver operating characteristic; AUC, area under curve.

superior longitudinal fasciculus were the WM fiber tracts which mainly suffered the severe damage in ADs. Inter-group classification was completed by SVM-RFE method. Multi-metrics combination would improve the classification performance compared with single diffusion metric. We also depicted the feature weighting distribution of WM tracts for each kind of DTI metric in order to research which WM fiber tract played an important role on classification.

In addition, the ROC curve and AUC could evaluate classifier output quality for each kind of diffusion metric.

There were several limitations to this research. First, small sample size would affect the reliability of classification results. Although our research used SVM model to distinguish AD group from HC group, it needed to be further verified on a larger sample to reinforce the current results and ensured that it had strong generalization ability. Deep learning could be combined if necessary. Another limitation was that the MCI group was absent from this study. MCI was known as a transition stage from health status to AD. It was necessary to include MCI in future studies to understand which features develop gradually over the course of the disease evolution and to reveal the degenerative pattern of the pathological mechanism of AD.

Availability of Data and Materials

The datasets generated and/or analyzed during the current study are available in the ADNI repository, http://adni.loni.usc.edu/.

Author Contributions

FZ designed the research study. YZ performed the research, analyzed the data and revised the manuscript. YZ and FZ wrote the manuscript. Both authors contributed to editorial changes in the manuscript. Both authors read and approved the final manuscript. Both authors have participated sufficiently in the work and agreed to be accountable for all aspects of the work.

Ethics Approval and Consent to Participate

The dataset we used was the public dataset of ADNI, the ethical approval was not required. In addition, informed written consent was obtained from all participants at every center.

Acknowledgment

We thank two anonymous reviewers for excellent criticism of the article.

Funding

This work was supported by the National Natural Science Foundation of China (Grant No.12202208), the Basic Science (Natural Science) Research Project of Colleges and Universities of Jiangsu Province (Grant No.22KJB310019, Grant No.22KJB130009), the Scientific Research Foundation of high-level personnel of Taizhou University (Grant No.TZXY2021QDJJ001), the Research and Cultivation Project for Young Teachers of Nanjing Audit University (Grant No.2021QNPY015), 2022 Double-Innovation Doctor of Jiangsu Province, "2022 Taizhou Tuo Ju Project" for Young science and Technology Talents, the Project of Excellent Science and Technology Innovation Team of Taizhou University.

Conflict of Interest

The authors declare no conflict of interest.

References

[1] Tiwari S, Atluri V, Kaushik A, Yndart A, Nair M. Alzheimer's disease: pathogenesis, diagnostics, and therapeutics. International Journal of Nanomedicine. 2019; 14: 5541–5554.

[2] Ferri CP, Prince M, Brayne C, Brodaty H, Fratiglioni L, Ganguli M, *et al*. Global prevalence of dementia: a Delphi consensus study. Lancet. 2005; 366: 2112–2117.

[3] 2020 Alzheimer's disease facts and figures. Alzheimer's & Dementia. 2020; 16: 391–460.

[4] Guzman-Martinez L, Calfío C, Farias GA, Vilches C, Prieto R, Maccioni RB. New Frontiers in the Prevention, Diagnosis, and Treatment of Alzheimer's Disease. Journal of Alzheimer's Disease. 2021; 82: S51–S63.

[5] Wang Z, Tang Z, Zhu Y, Pettigrew C, Soldan A, Gross A, *et al*. AD risk score for the early phases of disease based on unsupervised machine learning. Alzheimer's & Dementia. 2020; 16: 1524–1533.

[6] Pellegrini E, Ballerini L, Hernandez MDCV, Chappell FM, González-Castro V, Anblagan D, *et al*. Machine learning of neuroimaging for assisted diagnosis of cognitive impairment and dementia: A systematic review. Alzheimer's & Dementia. 2018; 10: 519–535.

[7] Zhutovsky P, Vijverberg EGB, Bruin WB, Thomas RM, Wattjes MP, Pijnenburg YAL, *et al*. Individual Prediction of Behavioral Variant Frontotemporal Dementia Development Using Multivariate Pattern Analysis of Magnetic Resonance Imaging Data. Journal of Alzheimer's Disease. 2019; 68: 1229–1241.

[8] Weiner MW, Veitch DP, Aisen PS, Beckett LA, Cairns NJ, Green RC, *et al*. Recent publications from the Alzheimer's Disease Neuroimaging Initiative: Reviewing progress toward improved AD clinical trials. Alzheimer's & Dementia. 2017; 13: e1–e85.

[9] Katabathula S, Wang Q, Xu R. Predict Alzheimer's disease using hippocampus MRI data: a lightweight 3D deep convolutional network model with visual and global shape representations. Alzheimer's Research & Therapy. 2021; 13: 104.

[10] Yan T, Wang Y, Weng Z, Du W, Liu T, Chen D, *et al*. Early-Stage Identification and Pathological Development of Alzheimer's Disease Using Multimodal MRI. Journal of Alzheimer's Disease. 2019; 68: 1013–1027.

[11] Roher AE, Weiss N, Kokjohn TA, Kuo Y, Kalback W, Anthony J, *et al*. Increased A beta peptides and reduced cholesterol and myelin proteins characterize white matter degeneration in Alzheimer's disease. Biochemistry. 2002; 41: 11080–11090.

[12] Amlien IK, Fjell AM. Diffusion tensor imaging of white matter degeneration in Alzheimer's disease and mild cognitive impairment. Neuroscience. 2014; 276: 206–215.

[13] Sjöbeck M, Haglund M, Englund E. White matter mapping in Alzheimer's disease: A neuropathological study. Neurobiology of Aging. 2006; 27: 673–680.

[14] Nasrabady SE, Rizvi B, Goldman JE, Brickman AM. White matter changes in Alzheimer's disease: a focus on myelin and oligodendrocytes. Acta Neuropathologica Communications. 2018; 6: 22.

[15] Parker TD, Slattery CF, Zhang J, Nicholas JM, Paterson RW, Foulkes AJM, *et al*. Cortical microstructure in young onset Alzheimer's disease using neurite orientation dispersion and density imaging. Human Brain Mapping. 2018; 39: 3005–3017.

[16] Torso M, Bozzali M, Zamboni G, Jenkinson M, Chance SA. Detection of Alzheimer's Disease using cortical diffusion tensor imaging. Human Brain Mapping. 2021; 42: 967–977.

[17] Le Bihan D, Mangin JF, Poupon C, Clark CA, Pappata S, Molko N, *et al*. Diffusion tensor imaging: concepts and applications. Journal of Magnetic Resonance Imaging. 2001; 13: 534–546.
[18] Basser PJ, Pierpaoli C. Microstructural and physiological features of tissues elucidated by quantitative-diffusion-tensor MRI. Journal of Magnetic Resonance. 2011; 213: 560–570.
[19] Basser PJ, Pierpaoli C. A simplified method to measure the diffusion tensor from seven MR images. Magnetic Resonance in Medicine. 1998; 39: 928–934.
[20] Smith SM, Jenkinson M, Johansen-Berg H, Rueckert D, Nichols TE, Mackay CE, *et al*. Tract-based spatial statistics: voxelwise analysis of multi-subject diffusion data. NeuroImage. 2006; 31: 1487–1505.
[21] Sheng J, Shao M, Zhang Q, Zhou R, Wang L, Xin Y. Alzheimer's disease, mild cognitive impairment, and normal aging distinguished by multi-modal parcellation and machine learning. Scientific Reports. 2020; 10: 5475.
[22] Ezzati A, Zammit AR, Harvey DJ, Habeck C, Hall CB, Lipton RB, *et al*. Optimizing Machine Learning Methods to Improve Predictive Models of Alzheimer's Disease. Journal of Alzheimer's Disease. 2019; 71: 1027–1036.
[23] Rohini M, Surendran D. Toward Alzheimer's disease classification through machine learning. Soft Computing. 2020; 25: 2589–2597.
[24] Lee JS, Kim C, Shin J, Cho H, Shin D, Kim N, *et al*. Machine Learning-based Individual Assessment of Cortical Atrophy Pattern in Alzheimer's Disease Spectrum: Development of the Classifier and Longitudinal Evaluation. Scientific Reports. 2018; 8: 4161.
[25] Cui Z, Xia Z, Su M, Shu H, Gong G. Disrupted white matter connectivity underlying developmental dyslexia: A machine learning approach. Human Brain Mapping. 2016; 37: 1443–1458.
[26] Dyrba M, Grothe M, Kirste T, Teipel SJ. Multimodal analysis of functional and structural disconnection in Alzheimer's disease using multiple kernel SVM. Human Brain Mapping. 2015; 36: 2118–2131.
[27] Oliveira PPDM, Nitrini R, Busatto G, Buchpiguel C, Sato JR, Amaro E. Use of SVM methods with surface-based cortical and volumetric subcortical measurements to detect Alzheimer's disease. Journal of Alzheimer's Disease. 2010; 19: 1263–1272.
[28] Yang B, Chen J, Chou W, Huang WS, Fuh JL, Liu RS, *et al*. Classification of Alzheimer's Disease from 18F-FDG and 11C-PiB PET Imaging Biomarkers Using Support Vector Machine. Journal of Medical and Biological Engineering. 2020; 40: 545–554.
[29] Veitch DP, Weiner MW, Aisen PS, Beckett LA, Cairns NJ, Green RC, *et al*. Understanding disease progression and improving Alzheimer's disease clinical trials: Recent highlights from the Alzheimer's Disease Neuroimaging Initiative. Alzheimer's & Dementia. 2019; 15: 106–152.
[30] Torso M, Ridgway GR, Hardingham I, Schwarz AJ, Chance SA. In Vivo Detection of Changes Related to Cortical Columnar Organization and Neuroinflammation Across the AD Continuum. The Journal of Prevention of Alzheimer's Disease. 2022; 9: 769–779.
[31] Beer JC, Tustison NJ, Cook PA, Davatzikos C, Sheline YI, Shinohara RT, *et al*. Longitudinal ComBat: A method for harmonizing longitudinal multi-scanner imaging data. NeuroImage. 2020; 220: 117129.
[32] Cui Z, Zhong S, Xu P, He Y, Gong G. PANDA: a pipeline toolbox for analyzing brain diffusion images. Frontiers in Human Neuroscience. 2013; 7: 42.
[33] Smith SM, Jenkinson M, Woolrich MW, Beckmann CF, Behrens TEJ, Johansen-Berg H, *et al*. Advances in functional and structural MR image analysis and implementation as FSL. NeuroImage. 2004; 23: S208–S219.
[34] Wang R, Benner T, Sorensen AG, Wedeen VJ. Diffusion Toolkit: A Software Package for Diffusion Imaging Data Processing and Tractography. Proc Intl Soc Mag Reson Med. 2007; 15: 3720.
[35] Bellec P, Lavoie-Courchesne S, Dickinson P, Lerch JP, Zijdenbos AP, Evans AC. The pipeline system for Octave and Matlab (PSOM): a lightweight scripting framework and execution engine for scientific workflows. Frontiers in Neuroinformatics. 2012; 6: 7.
[36] Mori S, Oishi K, Jiang H, Jiang L, Li X, Akhter K, *et al*. Stereotaxic white matter atlas based on diffusion tensor imaging in an ICBM template. NeuroImage. 2008; 40: 570–582.
[37] Abraham A, Pedregosa F, Eickenberg M, Gervais P, Mueller A, Kossaifi J, *et al*. Machine learning for neuroimaging with scikit-learn. Frontiers in Neuroinformatics. 2014; 8: 14.
[38] Furey TS, Cristianini N, Duffy N, Bednarski DW, Schummer M, Haussler D. Support vector machine classification and validation of cancer tissue samples using microarray expression data. Bioinformatics. 2000; 16: 906–914.
[39] Guyon I, Weston J, Barnhill S, Vapnik V. Gene Selection for Cancer Classification using Support Vector Machines. Machine Learning. 2002; 46: 34.
[40] Duan K, Rajapakse JC, Wang H, Azuaje F. Multiple SVM-RFE for gene selection in cancer classification with expression data. IEEE Transactions on Nanobioscience. 2005; 4: 228–234.
[41] Craddock RC, Holtzheimer PE, Hu XP, Mayberg HS. Disease state prediction from resting state functional connectivity. Magnetic Resonance in Medicine. 2009; 62: 1619–1628.
[42] De Martino F, Valente G, Staeren N, Ashburner J, Goebel R, Formisano E. Combining multivariate voxel selection and support vector machines for mapping and classification of fMRI spatial patterns. NeuroImage. 2008; 43: 44–58.
[43] Zhao M, Zhao C, Zheng C. Identifying Concealed Information Using Wavelet Feature Extraction and Support Vector Machine. Procedia Environmental Sciences. 2011; 8: 337–343.
[44] Zweig MH, Campbell G. Receiver-operating characteristic (ROC) plots: a fundamental evaluation tool in clinical medicine. Clinical Chemistry. 1993; 39: 561–577.
[45] Fawcett T. An introduction to ROC analysis. Pattern Recognition Letters. 2006; 27: 861–874.
[46] Xie S, Xiao JX, Gong GL, Zang YF, Wang YH, Wu HK, *et al*. Voxel-based detection of white matter abnormalities in mild Alzheimer disease. Neurology. 2006; 66: 1845–1849.
[47] Huang H, Fan X, Weiner M, Martin-Cook K, Xiao G, Davis J, *et al*. Distinctive disruption patterns of white matter tracts in Alzheimer's disease with full diffusion tensor characterization. Neurobiology of Aging. 2012; 33: 2029–2045.
[48] Agosta F, Pievani M, Sala S, Geroldi C, Galluzzi S, Frisoni GB, *et al*. White matter damage in Alzheimer disease and its relationship to gray matter atrophy. Radiology. 2011; 258: 853–863.
[49] Takahashi S, Yonezawa H, Takahashi J, Kudo M, Inoue T, Tohgi H. Selective reduction of diffusion anisotropy in white matter of Alzheimer disease brains measured by 3.0 Tesla magnetic resonance imaging. Neuroscience Letters. 2002; 332: 45–48.
[50] Stenset V, Bjørnerud A, Fjell AM, Walhovd KB, Hofoss D, Due-Tønnessen P, *et al*. Cingulum fiber diffusivity and CSF T-tau in patients with subjective and mild cognitive impairment. Neurobiology of Aging. 2011; 32: 581–589.
[51] Teipel SJ, Grothe MJ, Filippi M, Fellgiebel A, Dyrba M, Frisoni GB, *et al*. Fractional anisotropy changes in Alzheimer's disease depend on the underlying fiber tract architecture: a multiparametric DTI study using joint independent component analysis. Journal of Alzheimer's Disease. 2014; 41: 69–83.
[52] Catani M, Jones DK, Donato R, Ffytche DH. Occipito-temporal connections in the human brain. Brain. 2003; 126: 2093–2107.
[53] Mesulam MM. A cortical network for directed attention and unilateral neglect. Annals of Neurology. 1981; 10: 309–325.

[54] Rizzo M, Anderson SW, Dawson J, Nawrot M. Vision and cognition in Alzheimer's disease. Neuropsychologia. 2000; 38: 1157–1169.

[55] Wang Y, West JD, Flashman LA, Wishart HA, Santulli RB, Rabin LA, *et al*. Selective changes in white matter integrity in MCI and older adults with cognitive complaints. Biochimica Et Biophysica Acta. 2012; 1822: 423–430.

[56] Bozzali M, Falini A, Franceschi M, Cercignani M, Zuffi M, Scotti G, *et al*. White matter damage in Alzheimer's disease assessed in vivo using diffusion tensor magnetic resonance imaging. Journal of Neurology, Neurosurgery, and Psychiatry. 2002; 72: 742–746.

[57] Clark DL, Boutros NN, Mendez MF. The brain and behavior: an introduction to behavioral neuroanatomy. Journal of Neuropsychiatry. 2001; 13: 525–526.

[58] Hahn C, Lim H, Won WY, Ahn KJ, Jung W, Lee CU. Apathy and white matter integrity in Alzheimer's disease: a whole brain analysis with tract-based spatial statistics. PLoS ONE. 2013; 8: e53493.

[59] Torso M, Serra L, Giulietti G, Spanò B, Tuzzi E, Koch G, *et al*. Strategic lesions in the anterior thalamic radiation and apathy in early Alzheimer's disease. PLoS ONE. 2015; 10: e0124998.

[60] Head D, Buckner RL, Shimony JS, Williams LE, Akbudak E, Conturo TE, *et al*. Differential vulnerability of anterior white matter in nondemented aging with minimal acceleration in dementia of the Alzheimer type: evidence from diffusion tensor imaging. Cerebral Cortex. 2004; 14: 410–423.